Dissociative recombination and vibrational excitation of BF^+ in low energy electron collisions

2016 Plasma Sources Sci. Technol. 25 055022

(http://iopscience.iop.org/0963-0252/25/5/055022)

IOP Publishing Plasma Sources Science and Technology

Plasma Sources Sci. Technol. **25** (2016) 055022 (12pp) doi:10.1088/0963-0252/25/5/055022

Dissociative recombination and vibrational excitation of BF^+ in low energy electron collisions

J Zs Mezei[1,2,3,4], F Colboc[1], N Pop[5], S Ilie[1,5], K Chakrabarti[1,6], S Niyonzima[7], M Lepers[2], A Bultel[8], O Dulieu[2], O Motapon[9], J Tennyson[10], K Hassouni[4] and I F Schneider[1,2]

[1] Laboratoire Ondes et Milieux Complexes CNRS—Université du Havre—Université Normandie, 76058 Le Havre, France
[2] Laboratoire Aimé-Cotton, CNRS—Université Paris-Sud—ENS Cachan—Université Paris-Saclay, 91405 Orsay, France
[3] Institute of Nuclear Research of the Hungarian Academy of Sciences, PO Box 51, H-4001 Debrecen, Hungary
[4] Laboratoire des Sciences des Procédés et des Matériaux, CNRS—Université Paris 13—USPC, 93430 Villetaneuse, France
[5] Department of Fundamental of Physics for Engineers, Politehnica University of Timisoara, Bv. V. Parvan No. 2, 300223 Timisoara, Romania
[6] Dept. of Mathematics, Scottish Church College, 1 & 3 Urquhart Sq., Kolkata 700 006, India
[7] Département de Physique, Faculté des Sciences, Université du Burundi, B.P. 2700 Bujumbura, Burundi
[8] CORIA CNRS—Université de Rouen—Université Normandie, F-76801 Saint-Etienne du Rouvray, France
[9] LPF, UFD Mathématiques, Informatique Appliquée et Physique Fondamentale, University of Douala, PO Box 24157, Douala, Cameroon
[10] Dept. of Physics and Astronomy, University College London, London WC1E 6BT, UK

E-mail: janos.mezei@univ-lehavre.fr

Received 23 June 2016, revised 12 August 2016
Accepted for publication 19 August 2016
Published 12 September 2016

Abstract

The latest molecular data—potential energy curves and Rydberg-valence interactions—characterising the super-excited electronic states of BF are reviewed in order to provide the input for the study of their fragmentation dynamics. Starting from this input, the main paths and mechanisms of BF^+ dissociative recombination and vibrational excitation are analysed. Their cross sections are computed for the first time using a method based on the multichannel quantum defect theory (MQDT), and Maxwellian rate-coefficients are calculated and displayed in ready-to-be-used format for low temperature plasma kinetics simulations.

Keywords: non-equilibrium plasma, plasma immersion ion implantation, molecular cations, dissociative recombination, electron impact vibrational excitation, excited states, multichannel quantum defect theory

(Some figures may appear in colour only in the online journal)

1. Introduction

Boron fluoride (BF_3) containing plasmas are important for applications in the field of material processing. BF_3 and Ar/BF_3 plasmas are for instance used for *p*-type doping in the semi-conductor industry (Matsui *et al* 2004, Torregrosa *et al* 2004). Moreover, electrical discharges generated in complex mixture of BF_3 with nitrogen containing compounds have been proposed and investigated for the deposition of boron nitride coatings (Yu and Matsumoto 2003, Yamamoto *et al*

2006). All these processes make use of low pressure high density plasma sources where BF_3 interacts with the free electrons of the plasma through elastic and inelastic collisions. These collisions are not only the driver for the generation of the active key-species of the process, e.g. the positive ions for the plasma immersion ion implantation (PIII) doping processes or active radicals for the deposition processes, but they also contribute and govern the discharge equilibrium and stability through ionisation, attachment and recombination processes (Farber and Srivastava 1984, Kim and Irikura 2000, Agarwal and Kushner 2007). In particular, for high density magnetised inductively coupled radio-frequency sources used in many of these processes, the surface losses are limited due to the magnetic confinement, which makes the contribution of ion recombination and mutual recombination processes to the discharge equilibrium very significant. In this context, the BF^+ ion can represent a significant fraction of the ions produced when working at high power density discharge conditions for which BF_3 dissociation and dissociative ionisation are strongly enhanced and the plasma is dominated by BF_2 and BF fragments (Maury *et al* 2016). These species can therefore significantly contribute either as an active species in the processes or in the discharge ionisation-recombination equilibrium. The investigation of the dissociative recombination of BF^+ is therefore of importance for understanding BF_3 plasma processes.

The kinetic description of all the above mentioned environments is based on the knowledge of the rate coefficients of the dominant reactions, including those between electrons and molecular ions. As for the BF^+ ions, their abundance and their vibrational distribution are strongly affected by the dissociative recombination (DR),

$$BF^+(v_i^+) + e^- \rightarrow B + F, \tag{1}$$

and also by other competitive processes, such as inelastic collisions ($v_f^+ > v_i^+$) and super-elastic collisions ($v_f^+ < v_i^+$) which are also known as collisions of the second kind:

$$BF^+(v_i^+) + e^- \rightarrow BF^+(v_f^+) + e^-, \tag{2}$$

where v_i^+ and v_f^+ stand for the initial and final vibrational quantum number of the target ion, and rotational structure is neglected.

In the present work, we compute the DR and vibrational transition (VT)—vibrational excitation/de-excitation (VE/VdE)—cross sections and rate coefficients for the lowest three vibrational levels of the BF^+ in its ground electronic state using the multichannel quantum defect theory (MQDT). The paper is structured as follows: section 2 outlines the main ideas and steps of our MQDT approach. section 3 presents the molecular data used in the calculation. The main results are given in section 4 and the paper ends by conclusions.

2. The MQDT-type approach to DR

The MQDT approach (Giusti-Suzor 1980, Seaton 1983, Greene and Jungen 1985, Jungen 1996) has been shown to be a powerful method for the evaluation of the cross sections in collisions of electrons/photons with molecular cation/neutral systems. It was applied with great success in calculating DR cross sections to several diatomic systems like H_2^+ and its isotopologues (Giusti-Suzor *et al* 1983, Schneider *et al* 1991, Takagi 1993, Tanabe *et al* 1995, Schneider *et al* 1997, Amitay *et al* 1999), O_2^+ (Guberman and Giusti-Suzor 1991, Guberman 2000), NO^+ (Sun and Nakamura 1990, Vâlcu *et al* 1998, Schneider *et al* 2000b), LiH^+ (Čurík and Greene 2007), HeH^+ (Haxton and Greene 2009), $LiHe^+$ (Čurík and Gianturco 2013) and triatomics like H_3^+ (Schneider *et al* 2000a, Kokoouline *et al* 2001, Kokoouline and Greene 2003), and for its competitive processes like ro-vibrational transitions in case of NO^+ (Motapon *et al* 2006), CO^+ (Mezei *et al* 2015) and H_2^+ (Ngassam *et al* 2003b, Epée Epée *et al* 2015). Recently, a global version of MQDT (Jungen 2011) has been used to describe the photoabsorption, photoionisation and photodissociation of H_2 (Mezei *et al* 2012, 2014, Sommavilla *et al* 2016), providing very good agreement with highly accurate experimental results.

In the present paper, we use an MQDT-type method to study the electron-impact collision processes given by equations (1) and (2) which result from the quantum interference of the *direct* mechanism—the capture takes place into a dissociative state of the neutral system (BF^{**})—and the *indirect* one—the capture occurs *via* a Rydberg state of the molecule BF^* which is predissociated by the BF^{**} state. In both mechanisms the autoionization is in competition with the predissociation and leads, through the reaction (2), to *super-elastic collision* (SEC) ($v_i^+ > v_f^+$ in equation (2)), *elastic collision* (EC) ($v_i^+ = v_f^+$) and *inelastic collision* (IC) ($v_i^+ < v_f^+$).

A detailed description of our theoretical approach is given in previous studies (Little *et al* 2014, Mezei *et al* 2015). The major steps of the method only can be briefly outlined as follows:

(i) *Defining the interaction matrix* $\boldsymbol{\mathcal{V}}$:
Within a quasi-diabatic representation of the BF states, the interaction matrix is based on the computed (Chakrabarti and Tennyson 2009, Chakrabarti *et al* 2011) couplings between *ionisation* channels—associated to the vibrational levels v^+ of the cation and to the orbital quantum number l of the incident/Rydberg electron—and *dissociation* channels d_j.

(ii) *Computation of the reaction matrix* $\boldsymbol{\mathcal{K}}$:
Given $\boldsymbol{H_0}$ the Hamiltonian of the molecular system under study in which the Rydberg-valence interaction is neglected, we adopt the second-order perturbative solution for the Lippman–Schwinger integral equation (Florescu *et al* 2003, Ngassam *et al* 2003a, Motapon *et al* 2006), written in operatorial form as:

$$\boldsymbol{\mathcal{K}} = \boldsymbol{\mathcal{V}} + \boldsymbol{\mathcal{V}} \frac{1}{E - \boldsymbol{H_0}} \boldsymbol{\mathcal{V}}. \tag{3}$$

(iii) *Diagonalization of the reaction matrix,*
yields the corresponding eigenvectors and eigenvalues which are used to build the eigenchannel wavefunctions.

(iv) *Frame transformation from the Born–Oppenheimer (short-range) to the close-coupling (long-range) representation,*
relying, for a given electronic total angular momentum quantum number Λ and a given orbital quantum number of the incident/Rydberg electron l, on the quantum defect $\mu_l^{\Lambda}(R)$ and on the eigenvectors and eigenvalues of the K-matrix.

(v) *Construction of the generalised scattering matrix* $\boldsymbol{X}$,
based on the frame-transformation coefficients, this matrix being organised in blocks associated to open and/or closed (*o* and/or *c* respectively) channels:

$$\boldsymbol{X} = \begin{pmatrix} \boldsymbol{X}_{\mathbf{oo}} & \boldsymbol{X}_{\mathbf{oc}} \\ \boldsymbol{X}_{\mathbf{co}} & \boldsymbol{X}_{\mathbf{cc}} \end{pmatrix}. \tag{4}$$

(vi) *Construction of the generalised scattering matrix* $\boldsymbol{\mathcal{S}}$,

$$\boldsymbol{S} = \boldsymbol{X}_{\mathbf{oo}} - \boldsymbol{X}_{\mathbf{oc}} \frac{1}{\boldsymbol{X}_{\mathbf{cc}} - \exp(-\mathrm{i}2\pi\boldsymbol{\nu})} \boldsymbol{X}_{\mathbf{co}}. \tag{5}$$

Based on the open channels, the first term in equation (5), but also on their mixing with the closed ones, given by the second term, the denominator being responsible for the resonant patterns in the shape of the cross section (Seaton 1983). Here the matrix $\exp(-\mathrm{i}2\pi\boldsymbol{\nu})$ is diagonal and contains the effective quantum numbers ν_{v^+} associated to the vibrational thresholds of the closed ionisation channels.

(vii) *Computation of the cross-sections:*
For each of the relevant BF states, which are grouped by symmetry properties: electronic total angular momentum quantum number Λ, electronic spin singlet/triplet, and for a given target cation vibrational level v_{i}^+ and energy of the incident electron ε, the dissociative recombination and the vibrational excitation/de-excitation cross sections are computed using, respectively:

$$\sigma^{\mathrm{sym}}_{\mathrm{diss}\leftarrow v_{\mathrm{i}}^+} = \frac{\pi}{4\varepsilon}\rho^{\mathrm{sym}} \sum_{l,j} |S_{d_j,lv_{\mathrm{i}}^+}|^2, \tag{6}$$

$$\sigma^{\mathrm{sym}}_{v_{\mathrm{f}}^+\leftarrow v_{\mathrm{i}}^+} = \frac{\pi}{4\varepsilon}\rho^{\mathrm{sym}} \sum_{l,l'} |S_{l'v_{\mathrm{f}}^+,lv_{\mathrm{i}}^+} - \delta_{l'l}\delta_{v_{\mathrm{i}}^+v_{\mathrm{f}}^+}|^2, \tag{7}$$

where ρ^{sym} stands for the ratio between the multiplicity of the involved electronic states of BF and that of the target, BF^+.

3. Molecular data

The molecular data necessary to model the DR are the potential energy curve (PEC) of the ground state of the ion, the PECs of the neutral valence dissociative states interacting with the ionization continua, those of the Rydberg states associated to these continua below the threshold, and all the relevant Rydberg-valence couplings. These molecular data are mostly obtained from *ab initio* R-Matrix calculations. In order to extend the PECs to small and large values of the internuclear distance R, we used the quantum chemistry molecular data of Magoulas *et al* (2013).

3.1. ***Ab initio*** *R-Matrix calculations for the molecular states*

Ab initio R-matrix calculations of electron collision with the BF^+ ion yielding the relevant molecular data were performed by three of us (Chakrabarti and Tennyson 2009, Chakrabarti *et al* 2011). The R-matrix method is a state-of-the-art quantum scattering technique which can be used to calculate the properties of bound and resonant electronic states of a molecule (Tennyson 2010). The BF^+ target states were first obtained by performing a configuration interaction (CI) calculation. Subsequently this CI target wave function was used in an R-matrix calculation. The bound states of the BF molecule were obtained by searching for negative energy solutions using the BOUND program available within the R-Matrix code suite (Sarpal *et al* 1991, Carr *et al* 2012). This also produces quantum defects of the bound states. Resonances were detected and fitted to a Breit–Wigner profile (Tennyson and Noble 1984) to obtain their energies and widths. Subsequently the electronic couplings $V_{d_j,l}$ were obtained from the resonance widths $\Gamma_{d_j,l}$ using the relation

$$V_{d_j,l} = \sqrt{\frac{\Gamma_{d_j,l}}{2\pi}}. \tag{8}$$

The calculations were repeated for 11 internuclear distances in the range $1.5\ a_0 - 3.5\ a_0$. While the R-matrix calculations used several partial waves to represent the scattering, one single *global* (i.e. not *l*-resolved) resonance width was produced for each symmetry. Consequently, one generic partial wave for each symmetry, corresponding to the highest effective quantum number produced by the R-matrix computation (see figure 3 from Chakrabarti *et al* (2011)), was considered to take in charge the total strength of the Rydberg-valence interaction in the current calculations. Dissociative curves were constructed using the resonance data above the ion PEC and their continuation as bound states below the ion PEC.

3.2. *Modeling of the potential energy curves and electronic couplings*

Our earlier studies on molecular systems such as H_2 (Epée Epée *et al* 2015), HD (Motapon *et al* 2014), NO (Motapon *et al* 2006), N_2 (Little *et al* 2014) and CO (Mezei *et al* 2015) revealed that accurate and complementary R-matrix and quantum chemistry calculations are needed for a reliable description of the molecular dynamics in electron/molecular cation collisions. In particular, we found that the DR cross section is extremely sensitive to the position of the PECs of the neutral dissociative states with respect to that of the target ion. Indeed, a slight change of the crossing point of the PEC of a neutral dissociative state with that of the ion ground state can lead to a significant change in the predicted DR cross section. In addition, the PECs of the dissociative states must also go to the correct asymptotic limits for large values of the internuclear distance R.

In order to fulfil these accuracy criteria, we smoothly matched the PECs corresponding to R-matrix resonances, situated above the ion PEC, to branches of adiabatic PECs coming from previous quantum chemistry calculations

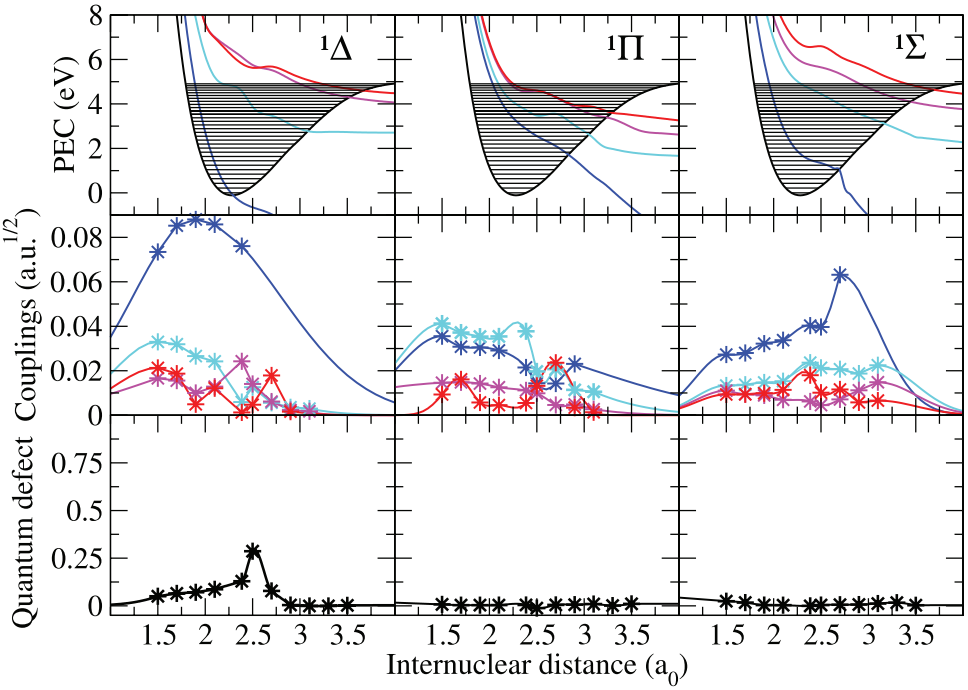

Figure 1. The dissociative states, electronic couplings and quantum defects relevant for BF^+ dissociative recombination within the major symmetries, indicated in each figure. Top panel: the potential energy curves of the dissociative BF^{**} states (colour, see section 3), the ground state potential energy curve of BF^+ and its vibrational levels (black). Mid panel: couplings between the valence BF^{**} dissociative states and the ionisation continua $BF^+ + e^-$. Bottom panel: quantum defects characterising the Rydberg series for the given symmetry. The symbols stand for the R-matrix data points.

(Magoulas *et al* 2013). Some of these latter PECs allowed us to complete the relevant diabatic landscape. More specifically, since for the states having $^1\Sigma^+$ and $^1\Pi$ symmetry the avoided crossings involved always two adiabatic states only, the adiabatic PECs can be a transformed into (quasi-)diabatic PECs using a 2×2 rotation matrix (Roos *et al* 2009). Meanwhile, far from the avoided crossing, we assumed that the adiabatic and diabatic potential curves are identical. This assumption forces the rotational angle to be a function that varies steeply from 0 to $\pi/2$, chosen in the present case a tangent hyperbolic function. In this way we were able to extract the diabatic PECs for the dissociative states with singlet symmetries relevant for DR.

The electronic couplings provided by the R-matrix theory (Chakrabarti *et al* 2011) for the triplet states are at least one or even two orders of magnitude smaller then those of the singlet ones, so they are omitted in the present calculation.

The data on the PECs are limitted to internuclear distances with $R \leqslant 8$ a$_0$. We completed the diabatic PECs by adding a long-range tail of $D - \sum_n C_n/R^n$ type (Stone 1996, Lepers and Dulieu 2011) for larger values of R, where D is the dissociation limit as given in the Kramida *et al* (2015). For the ground state of BF^+, the leading term C_3/R^3 of the multipolar expansion comes from the interaction between the charge of B^+ and the quadrupole moment of fluorine in its ground state $^2P^o(M_L = 0)$, with M_L the azimuthal quantum number of F with respect to the internuclear axis. The corresponding coefficient $C_3 = Q = 0.731$ a.u. Medved *et al* (2000) gives rise to a repulsive interaction, which is balanced by the next term C_4/R^4 of the multipolar expansion, due to the polarisation of the electronic cloud of F by the ion B^+. The coefficient is given by $C_4 = -\alpha_{zz}/2 = -1.72$ a.u., where $\alpha_{zz} = 3.43$ a.u. (Medved *et al* 2000) is the static dipole polarisability of the ground state $^2P^o(M_L = 0)$ of fluorine. As for the states of the BF, the C_n coefficients are calculated as fitting parameters to ensure a smooth connection with the existing part of the PECs.

The top panel of figure 1 shows the PEC of the ion ground state—together with its vibrational structure—and the PECs of the DR-relevant dissociative states obtained using the procedure outlined above and taken into account in the present MQDT calculation. The electronic couplings of these latter states with the ionization continua, computed from the R-Matrix-produced autoionization widths followed by Gaussian-type extrapolations to small and large internuclear distances, are shown in the mid panel of the same figure. The bottom panel gives the quantum defects characterising the Rydberg series for the different symmetries. They are small in absolute value and slowly variable with the internuclear distance R, with a notable exception in a small region around 2.5 a$_0$ in the case of the $^1\Delta$ symmetry, due to local relatively strong Rydberg-valence interactions.

4. Results and discussion

4.1. Evaluation of the cross section using the MQDT approach

Using the set of molecular data (PECs, electronic couplings and quantum defects) determined as described in the previous section, we performed a series of MQDT calculations of cross sections for DR and competitive processes, assuming BF^+ to

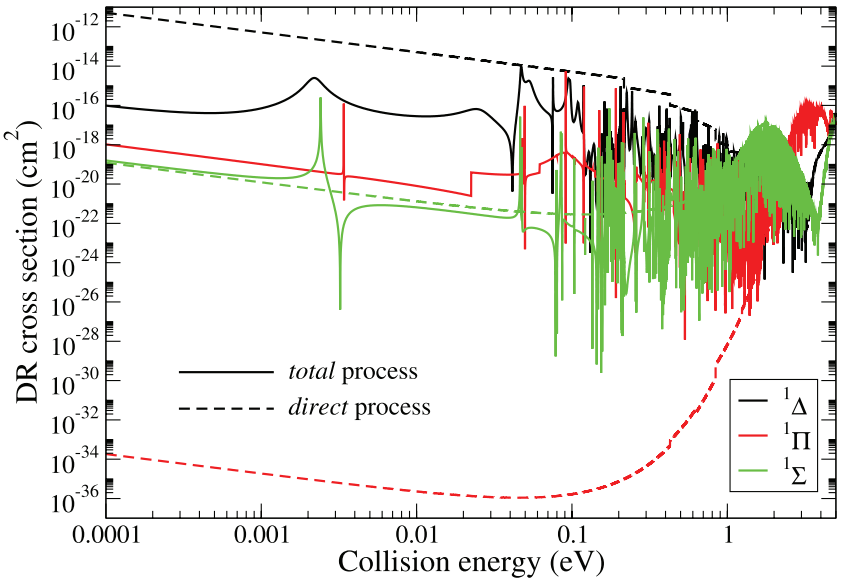

Figure 2. DR cross section for the direct (dashed lines) and the total (direct and indirect) processes (continuous lines) for each symmetry, with the ion initially in $v_i^+ = 0$.

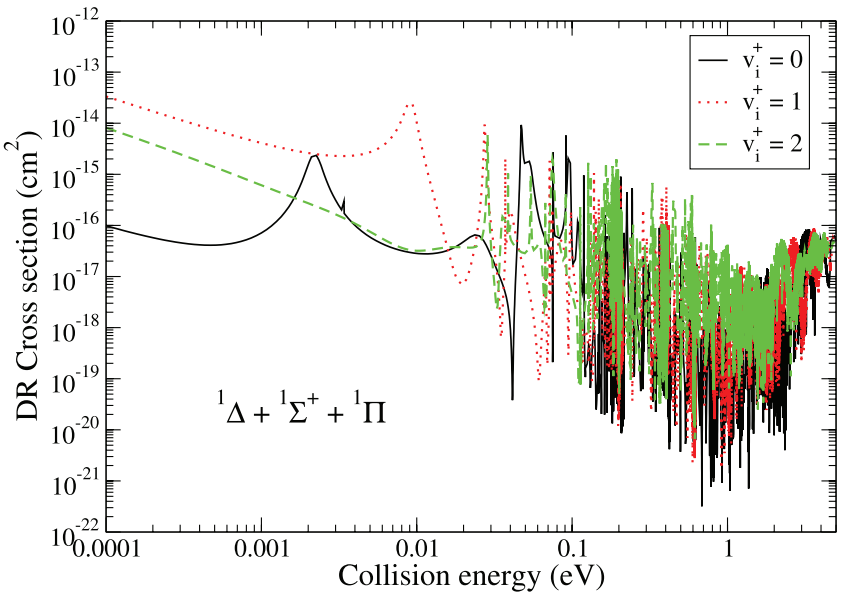

Figure 3. Total DR cross sections for different initial vibrational levels of the ion, for all of the symmetries considered. Black continuous lines are for DR from $v_i^+ = 0$, while the red dotted and green dashed lines are for DR from $v_i^+ = 1$ and 2, respectively.

be initially in its electronic ground state X $^2\Sigma^+$ and on one of its lowest vibrational levels $v_i^+ = 0, 1$ and 2. We have considered that the reactive processes take place via BF-states of total symmetry of $^1\Delta$, $^1\Pi$, $^1\Sigma^+$—see figure 1—and we neglected rotational and spin-orbit effects.

We consider incident electron energies from 0.01 meV up to 5 eV—the dissociation energy of BF^+ X $^2\Sigma^+$ electronic state—and all the 30 vibrational levels of the ion are included in the calculations.

At very low energy, all the excited levels are associated with closed ionisation channels, as defined in section 2, responsible for temporary resonant capture into Rydberg states. As the energy increases, more and more ionisation channels open, which results in autoionization, leading to competitive processes, such as IC and SEC, and decreasing the flux of DR.

The direct electronic couplings between ionisation and dissociation channels—mentioned in paragraph (i) of section 2—were extracted from the autoionization widths (see equation (8)) of the valence states calculated by Chakrabarti and Tennyson (2009). For each dissociation channel available, we considered interaction with the most relevant series of Rydberg states including only one partial wave for each symmetry.

By examining the magnitude of the valence-Rydberg couplings (shown in the middle panel of figure 1) and the positions of the crossing points between the dissociative states correlating to the $B(2p^1) + F(2p^5)$ atomic limits with the ionic ground state—blue and black curves in the first figure of the upper panel of the same figure—at low collision energies (up to 1 eV) one may predict that the major

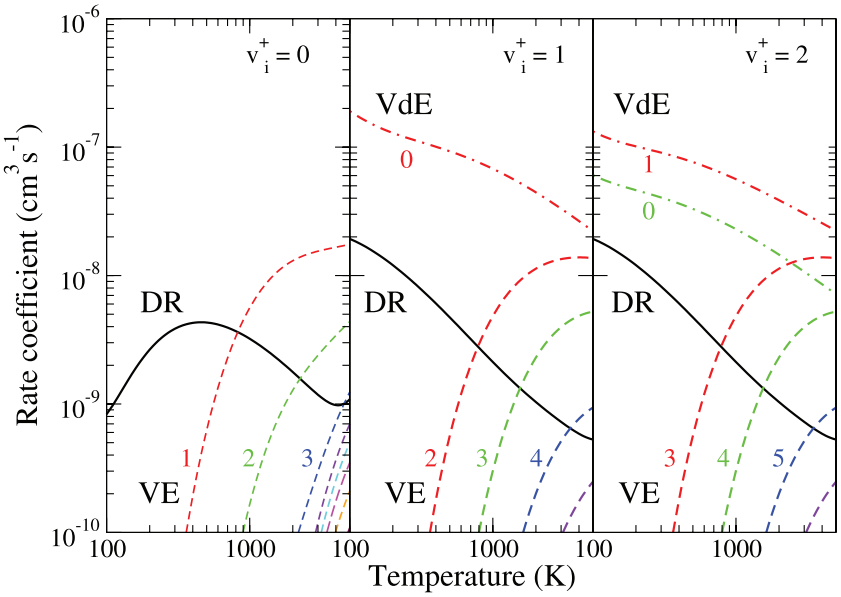

Figure 4. DR and state-to-state VE and VdE Maxwell rate coefficients of BF^+ in its ground electronic state, v_i^+ standing for the initial vibrational quantum number of the target ion. Curves of the same color show the rate coefficients for the vibrational (de-)excitations corresponding to the same $|\Delta v| = |v_f^+ - v_i^+|$; $v_f^+ > v_i^+$ for the VE and $v_f^+ < v_i^+$ for the VdE global rate coefficients. The final vibrational quantum numbers of the ion are indicated for these processes.

part of the total cross section comes from the $^1\Delta$ symmetry (solid black line in figure 2), while the $^1\Sigma$ and $^1\Pi$ symmetries (solid green and red lines in the same figure) only make a minor contribution to the cross section. The importance of these latter two symmetries is revealed at higher collision energies, when the crossing of the first dissociative state with the molecular ion becomes favorable. At collision energies about 1 eV, the $^1\Sigma^+$ states give a larger contribution to the DR cross section than the $^1\Delta$ symmetry, which in turn is exceeded by the $^1\Pi$ symmetry at about 2 eV. Moreover, one can notice that at higher collision energies, around 3.5 eV, when all the dissociative states are open, the DR cross section shows a sharp revival and, at 5 eV, the resonance structures disappear since all the ionization channels are open, and consequently the direct process only drives the DR.

Figure 2 shows the importance of the *indirect* process for the DR of vibrationally relaxed BF^+ at low energies.

Within the $^1\Delta$ symmetry, the entrance ionization channel associated with the $v_i^+ = 0$ state is strongly coupled to the dissociation continuum (see figure 1), allowing the direct process to dominate. The indirect process diminishes the cross section— *destructive* interferences with the direct one—due to stronger coupling between closed channels associated with highly-excited vibrational levels—$v^+ = 12$–16—and the dissociative ones.

Within the $^1\Pi$ symmetry one finds the opposite. The direct process gives only a minor contribution to the DR cross section, due to the poor Franck–Condon overlap between the vibrational wave function of the initial state of the ion and the dissociative neutral states. However, the much stronger couplings between some closed ionisation channels—$v^+ = 8$–10—and the dissociative states significantly increases the total cross section through the indirect mechanism (Pop *et al* 2012, Schneider *et al* 2012) resulting into *constructive* quantum interferences.

Finally, for the states with $^1\Sigma^+$ symmetry, the indirect process plays a relatively minor role, the magnitude of the total cross section being given mainly by the direct process. The indirect process is responsible for resonant structures which are a consequences of both constructive and destructive interference.

For a given initial vibrational level of BF^+, the total DR cross section is obtained by summing over the partial cross sections of the three symmetries contributing to the process—$^1\Delta$, $^1\Pi$ and $^1\Sigma^+$—given in equation (6). The results of the calculations performed for the lowest three vibrational levels of the ground electronic state of the ion are shown in figure 3.

4.2. Reaction rate coefficients for DR and its competitive processes

Besides the dissociative recombination cross sections presented in figure 3, we use equation (7) to calculate the vibrational excitation (VE) and de-excitation (VdE) cross sections for the same vibrational levels of the target. Since many of the features of the VE and VdE cross sections either are similar to, or may be understood with the same reasoning as those of DR, we do not display them here. Instead, we present in this section their Maxwell rate coefficients for a broad range of electronic temperatures, in comparison with those of the DR. All these data are relevant for cold non-equilibrium plasmas.

Figure 4 shows the total DR and vibrational transition—VE and VdE—rate coefficients for the three lowest vibrational levels of the ion. The DR rate for $v_i^+ = 0$ shows different behaviour to those for the $v_i^+ = 1$ and 2 states. It has a maximum at an

Table 1. Parameters used in equation (9) to represent the DR rate coefficient of BF^+.

v	A_v	α_v	$B_v(1)$	$B_v(2)$	$B_v(3)$	$B_v(4)$	$B_v(5)$	$B_v(6)$	$B_v(7)$
0	0.703 050 632[−5]	−0.108 298 227[1]	−0.363 984 388[2]	0.685 227 53[6]	−0.341 534 791[9]	0.862 623 62[11]	−0.117 919 938[14]	0.821 543 800[15]	−0.229 194 862[17]
1	0.205 402 433[−11]	0.557 133 316[0]	−0.185 580 405[4]	0.110 399 946[7]	−0.316 387 400[9]	0.531 242 790[11]	−0.525 109 108[13]	0.283 203 635[15]	−0.643 843 159[16]
2	0.144 845 145[−5]	−0.806 777 388[0]	0.285 629 778[4]	−0.322 036 339[7]	0.160 926 033[10]	−0.409 338 097[12]	0.558 087 964[14]	−0.388 815 002[16]	0.108 682 270[18]

Note: Powers of 10 are given in square brackets.

Table 2. Parameters used in equation (10) to represent the VE rate coefficient of BF^+ ($v = 0$).

$v' \to v''$	T_{min}(K)	$A_{v' \to v''}$	$\alpha_{v' \to v''}$	$B_{v' \to v''}(1)$	$B_{v' \to v''}(2)$	$B_{v' \to v''}(3)$	$B_{v' \to v''}(4)$	$B_{v' \to v''}(5)$	$B_{v' \to v''}(6)$	$B_{v' \to v''}(7)$
$0 \to 1$	100	0.262 533 924[−5]	−0.547 999 875[0]	0.214 096 395[4]	0.639 318 590[6]	−0.338 435 157[9]	0.871 079 196[11]	−0.119 891 991[14]	0.844 485 990[15]	−0.238 785 179[17]
$0 \to 2$	250	0.173 038 633[−11]	0.899 303 013[0]	−0.154 506 863[4]	0.103 113 831[8]	−0.802 809 891[10]	0.345 037 537[13]	−0.831 154 448[15]	0.104 995 341[18]	−0.541 063 017[19]
$0 \to 3$	350	0.228 322 632[−19]	0.298 753 871[1]	0.362 608 159[4]	−0.187 052 923[8]	0.462 415 666[11]	−0.437 428 769[14]	0.208 086 587[17]	−0.496 004 570[19]	0.471 734 143[21]
$0 \to 4$	500	0.117 098 647[13]	−0.484 209 878[1]	0.440 674 967[5]	−0.535 140 469[8]	−0.648 699 676[9]	0.669 344 086[14]	−0.628 654 524[17]	0.237 907 644[20]	−0.333 577 789[22]
$0 \to 5$	700	0.409 903 965[−3]	−0.115 252 435[1]	0.195 259 810[5]	−0.556 269 189[7]	0.845 592 131[10]	−0.259 895 652[14]	0.300 647 776[17]	−0.147 809 013[20]	0.269 130 250[22]
$0 \to 6$	1000	0.208 106 654[−4]	−0.886 590 160[0]	0.164 181 737[5]	0.130 228 539[8]	−0.448 925 166[11]	0.652 593 625[14]	−0.524 133 410[17]	0.227 101 018[20]	−0.413 751 683[22]
$0 \to 7$	1000	0.191 744 424[−4]	−0.916 885 978[0]	0.176 354 084[5]	0.715 839 067[7]	−0.242 161 884[11]	0.338 962 077[14]	−0.251 630 983[17]	0.96444.8872[19]	−0.147 532 452[22]

Note: Powers of 10 are given in square brackets.

Table 3. Parameters used in equation (10) to represent the VE rate coefficient of BF^+ ($v = 1$).

$v' \to v''$	T_{min}(K)	$A_{v' \to v''}$	$\alpha_{v' \to v''}$	$B_{v' \to v''}(1)$	$B_{v' \to v''}(2)$	$B_{v' \to v''}(3)$	$B_{v' \to v''}(4)$	$B_{v' \to v''}(5)$	$B_{v' \to v''}(6)$	$B_{v' \to v''}(7)$
$1 \to 0$	100	0.452 471 923[−4]	−0.870 739 533[0]	0.482 355 385[3]	−0.159 745 070[6]	0.206 190 286[8]	−0.357 598 119[9]	−0.236 882 495[12]	0.278 880 714[14]	−0.100 143 557[16]
$1 \to 2$	100	0.206 894 707[−4]	−0.534 102 059[0]	0.240 138 665[4]	0.240 026 523[6]	−0.118 750 781[9]	0.294 642 142[11]	−0.398 661 667[13]	0.277 400 105[15]	−0.775 646 365[16]
$1 \to 3$	500	0.132 913 428[3]	−0.796 311 915[0]	0.528 489 192[4]	−0.227 298 093[6]	0.992 018 062[8]	−0.246 177 290[11]	0.334 949 142[13]	−0.234 694 329[15]	0.661 421 602[16]
$1 \to 4$	1000	0.618 690 809[−3]	−0.105 997 410[1]	0.102 015 058[5]	−0.102 556 918[8]	0.227 295 645[11]	−0.322 366 448[14]	0.285 015 517[17]	−0.142 527 673[20]	0.306 796 130[22]
$1 \to 5$	1000	0.195 393 605[−5]	−0.554 467 702[0]	0.874 898 467[4]	0.410 394 065[7]	−0.950 355 092[10]	0.129 851 249[14]	−0.110 278 414[17]	0.546 465 683[19]	−0.120 534 084[22]
$1 \to 6$	1500	0.144 480 570[27]	−0.772 731 693[1]	0.121 808 074[6]	−0.696 758 177[9]	0.243 696 228[13]	−0.508 560 332[16]	0.633 554 530[19]	−0.436 110 956[22]	0.127 890 210[25]

Note: Powers of 10 are given in square brackets.

Table 4. Parameters used in equation (10) to represent the VE rate coefficient of BF^+ ($v = 2$).

$v' \to v''$	$T_{\min}$(K)	$A_{v'\to v''}$	$\alpha_{v'\to v''}$	$B_{v'\to v''}(1)$	$B_{v'\to v''}(2)$	$B_{v'\to v''}(3)$	$B_{v'\to v''}(4)$	$B_{v'\to v''}(5)$	$B_{v'\to v''}(6)$	$B_{v'\to v''}(7)$
$2 \to 0$	100	0.206 905 711[−4]	−0.534 094 193[0]	−0.522 292 591[2]	0.239 747 229[6]	−0.118 624 395[9]	0.294 301 198[11]	0.235 044 551[13]	0.277 059 236[15]	−0.774 678 282[16]
$2 \to 1$	100	0.281 749 676[−3]	−0.939 661 066[0]	0.573 963 533[3]	−0.266 713 211[6]	0.925 188 414[8]	−0.195 045 354[11]	−0.831 154 448[15]	−0.149 951 574[15]	0.392 910 054[16]
$2 \to 3$	200	0.677 540 315[−6]	−0.180 526 927[0]	0.165 713 437[4]	0.786 441 694[6]	−0.355 111 141[9]	0.865 145 438[11]	−0.110 403 668[14]	0.586 781 113[15]	−0.159 145 807[16]
$2 \to 4$	500	0.312 513 647[−2]	−0.113 354 017[1]	0.791 543 066[4]	−0.692 210 036[7]	0.883 457 770[10]	−0.684 463 255[13]	0.319 179 702[16]	−0.822 026 586[18]	0.896 873 812[20]
$2 \to 5$	1000	0.641 993 202[−3]	−0.101 279 417[1]	0.931 521 134[4]	−0.338 959 607[7]	0.140 747 992[10]	0.325 809 186[13]	−0.558 558 120[16]	0.350 923 558[19]	−0.820 376 383[21]

Note: Powers of 10 are given in square brackets.

electron temperature T_e of about 400 K, while the rates for the other two states are monotonically decreasing with T_e, reaching nearly the same magnitude at higher temperatures. This behaviour for $v_i^+ = 0$ comes from the strong resonant peaks just below 0.01 eV, see figure 2 and black curve in figure 3.

For other recently studied molecular systems, N_2 (Little *et al* 2014) and CO (Mezei *et al* 2015), the DR clearly dominates the electron-ion collisions. However, for BF the calculated VdE rate coefficients are larger than the DR-ones, and VE rate coefficients exceed the DR-ones at high T_e by almost an order of magnitude. Thus, one can conclude that in the case of the BF^+ containing plasma, the internal vibrational energy is much more important for energy-exchange via VE and VdE, than the kinetic energy release via the exothermic DR.

To facilitate the use of our rate coefficients (figure 4) in modeling calculations, we fit them using modified Arrhenius-type formulas. The calculated DR rate coefficients for $v = 0$, 1, 2 are given by :

$$k^{\mathrm{DR}}_{\mathrm{BF}^+,v}(T_e) = A_v T_e^{\alpha_v} \exp\left[-\sum_{i=1}^{7} \frac{B_v(i)}{i \cdot T_e{}^i}\right] \qquad (9)$$

over the electron temperature range $100\,\mathrm{K} < \mathrm{T_e} < 3000\,\mathrm{K}$. The parameters A_v, α_v, and $\mathrm{B}_v(\mathrm{i})$ are listed in table 1. The corresponding formula for the vibrational transitions (VE and VdE) has the form:

$$k^{\mathrm{DR}}_{\mathrm{BF}^+,v'\to v''}(T_e) = A_{v'\to v''} T_e^{\alpha_{v'\to v''}} \exp\left[-\sum_{i=1}^{7} \frac{B_{v'\to v''}(i)}{i \cdot T_e{}^i}\right] \qquad (10)$$

over the electron temperature range $\mathrm{T_{min}} < \mathrm{T_e} < 3000\,\mathrm{K}$. The parameters $\mathrm{T_{min}}$, $A_{v'\to v''}$, $\alpha_{v'\to v''}$, and $B_{v'\to v''}(i)$ for $i = 1, 2, \ldots, 7$ are given in tables 2–4.

5. Conclusion

This paper presents a theoretical study of the dissociative recombination of BF^+ and of its competitive processes—vibrational excitation and de-excitation—over a broad range of electron energies—up to about 5 eV—and considering all the relevant dissociative states within different symmetries. Our MQDT dynamical approach is relying on molecular data calculated by the *ab initio* R-matrix method, completed by quantum chemical results. The computed Maxwell rate coefficients are relevant for the kinetic modelling of molecule based cold non-equilibrium plasmas, in the context of complete lack of other theoretical or experimental data on these processes for this cation.

The present calculations complete our very recent studies of the DR performed on N_2^+ (Little *et al* 2014) and on CO^+ (Mezei *et al* 2015) based on fully *ab initio* potential energy curves and couplings computed with the R-matrix method (Tennyson 2010), since BF^+ is isoelectronic with these two molecular systems. We note that while there is no experimental data available for the processes considered here for BF^+, our previous calculation on N_2^+ and CO^+ gave good agreement with the available measurements.

Acknowledgments

The authors acknowledge support from the International Atomic Energy Agency (IAEA, Vienna) via the Coordinated Research Project 'Light Element Atom, Molecule and Radical Behaviour in the Divertor and Edge Plasma Regions', from the French Agence Nationale de la Recherche via the projects 'SUMOSTAI' (No. ANR-09-BLAN-020901) and 'HYDRIDES' (No. ANR-12-BS05-0011-01), from the IFRAF-Triangle de la Physique via the project 'SpecoRyd', and from the Centre National de la Recherche Scientifique via the programs 'Physique et Chimie du Milieu Interstellaire', the PEPS project TPCECAM and the GdR ThéMS. They also acknowledge generous financial support from Région Haute-Normandie via the CPER, GRR Electronique, Energie et Matériaux and BIOENGINE project, from the 'Fédérations de Recherche 'Energie, Propulsion, Environnement' and 'Fusion par Confinement Magnétique' ITER, and from the LabEx EMC^3, via the project PicoLIBS (No. ANR-12-BS05-0011-01). KC thanks the Institut des Sciences de l'Ingénierie et des Systèmes (INSIS) of CNRS for a research grant in 2013, and the Laboratoire Ondes et Matériaux Complexes (LOMC) of Le Havre University for hospitality. SI, NP and IFS acknowledge EU for financial support via the ERASMUS convention between Le Havre University and Politehnica University of Timisoara. FC and IFS acknowledge EU for financial support via the ERASMUS convention between Le Havre University and University College London and the COST action 'Our Astrochemical History'.

References

Agarwal A and Kushner M 2007 *J. Appl. Phys.* **101** 063305
Amitay Z *et al* 1999 *Phys. Rev.* A **60** 3769
Carr J M, Galiatsatos P G, Gorfinkiel J D, Harvey A G, Lysaght M A, Madden D, Masin Z, Plummer M and Tennyson J 2012 *Eur. Phys. J.* D **66** 58
Chakrabarti K and Tennyson J 2009 *J. Phys. B: At. Mol. Opt. Phys.* **42** 105204
Chakrabarti K, Schneider I F and Tennyson J 2011 *J. Phys. B: At. Mol. Opt. Phys.* **44** 055203
Čurík R and Gianturco F A 2013 *Phys. Rev.* A **87** 012705
Čurík R and Greene C H 2007 *Phys. Rev. Lett.* **98** 173201
Epée Epée M D, Mezei J Zs, Motapon O, Pop N and Schneider I F 2015 *Mon. Not. R. Astron. Soc.* **455** 276
Farber M and Srivastava R D 1984 *J. Chem. Phys.* **81** 241–4
Florescu A I, Ngassam V, Schneider I F and Suzor-Weiner A 2003 *J. Phys. B: At. Mol. Opt. Phys.* **36** 1205
Giusti-Suzor A 1980 *J. Phys. B: At. Mol. Phys.* **13** 3867
Giusti-Suzor A, Bardsley J N and Derkits C 1983 *Phys. Rev.* A **28** 682–91
Greene C H and Jungen Ch 1985 *Adv. At. Mol. Phys.* **21** 51
Guberman S L 2000 *Dissociative Recombination: Theory, Experiment and Applications IV* ed M Larsson *et al* (Singapore: World Scientific) pp 1–11
Guberman S L and Giusti-Suzor A 1991 *J. Chem. Phys.* **95** 2602
Haxton D J and Greene C H 2009 *Phys. Rev.* A **79** 022701
Jungen Ch (ed) 1996 *Molecular Applications of Quantum Defect Theory* (Bristol: Institute of Physics Publishing)
Jungen Ch 2011 Elements of quantum defect theory *Handbook of High Resolution Spectroscopy* ed M Quack and F Merkt (Chichester: Wiley)

Kim Y-K and Irikura K 2000 *AIP Conf. Proc.* **543** 220
Kokoouline V and Greene C H 2003 *Phys. Rev.* A **68** 012703
Kokoouline V, Greene C H and Esry B D 2001 *Nature* **412** 891
Kramida O, Ralchenko Yu, Reader J and NIST ASD Team 2015 *NIST Atomic Spectra Database (ver. 5.3)* (Gaithersburg, MD: National Institute of Standards and Technology) (http://physics.nist.gov/asd)
Lepers M and Dulieu O 2011 *Eur. Phys. J.* D **65** 113
Little D A, Chakrabarti K, Mezei J Zs, Schneider I F and Tennyson J 2014 *Phys. Rev.* A **90** 052705
Magoulas I, Kalemos A and Mavridis A 2013 *J. Chem. Phys.* **138** 104312
Matsui T, Kondo M and Matsuda A 2004 *J. Non-Cryst. Solids* **338** 646–50
Maury M, Torregrosa F, Borvon G and Hassouni K 2016 to be submitted to *Plasma Chem. Plasma Process.*
Medved M, Fowler P W and Hutson J M 2000 *Mol. Phys.* **98** 453
Mezei J Zs *et al* 2015 *Plasma Sources Sci. Technol.* **24** 035005
Mezei J Zs, Schneider I F, Glass-Maujean M and Jungen Ch 2014 *J. Chem. Phys.* **141** 064305
Mezei J Zs, Schneider I F, Roueff E and Jungen Ch 2012 *Phys. Rev.* A **85** 043411
Motapon O, Fifirig M, Florescu A, Waffeu Tamo F O, Crumeyrolle O, Varin-Bréant G, Bultel A, Vervisch P, Tennyson J and Schneider I F 2006 *Plasma Sources Sci. Technol.* **15** 23
Motapon O, Pop N, Argoubi F, Mezei J Zs, Epee Epee M D, Faure A, Telmini M, Tennyson J and Schneider I F 2014 *Phys. Rev.* A **90** 012706
Ngassam V, Florescu A, Pichl L, Schneider I F, Motapon O and Suzor-Weiner A 2003a *Eur. Phys. J.* D **26** 165
Ngassam V, Motapon O, Florescu A, Pichl L, Schneider I F and Suzor-Weiner A 2003b *Phys. Rev.* A **68** 032704
Pop N, Lique F and Schneider I F 2012 *AIP Conf. Proc.* **1472** 162
Roos J B, Orel A E and Larson Å 2009 *Phys. Rev.* A **79** 062510
Sarpal B K, Branchett S E, Tennyson J and Morgan L A 1991 *J. Phys. B: At. Mol. Opt. Phys.* **24** 3685–99
Schneider I F, Dulieu O and Giusti-Suzor A 1991 *J. Phys. B: At. Mol. Phys.* **24** L289
Schneider I F, Orel A E and Suzor-Weiner A 2000a *Phys. Rev. Lett.* **85** 3785
Schneider I F, Pop N and Jungen Ch 2012 *Phys. Rev.* A **86** 062706
Schneider I F, Rabadan L I, Carata L, Tennyson J, Andersen A H and Suzor-Weiner A 2000b *J. Phys. B: At. Mol. Opt. Phys.* **33** 4849
Schneider I F, Strömholm C, Carata L, Urbain X, Larsson M and Suzor-Weiner A 1997 *J. Phys. B: At. Mol. Opt. Phys.* **30** 2687
Seaton M J 1983 *Rep. Prog. Phys.* **46** 167
Sommavilla M, Merkt F, Mezei J Zs and Jungen Ch 2016 *J. Chem. Phys.* **144** 084303
Stone A J 1996 *The Theory of Intermolecular Forces* (New York: Oxford University Press)
Sun H and Nakamura H 1990 *J. Chem. Phys.* **93** 6491
Takagi H 1993 *J. Phys. B: At. Mol. Opt. Phys.* **26** 4815
Tanabe T *et al* 1995 *Phys. Rev. Lett.* **75** 1066
Tennyson J 2010 *Phys. Rep.* **491** 29–76
Tennyson J and Noble C J 1984 *Comput. Phys. Commun.* **33** 421–4
Torregrosa F, Laviron C, Faik H, Barakel D, Milesi F and Baccaccia S 2004 *Surf. Coat. Technol.* **186** 93–8
Vâlcu B, Schneider I F, Raoult M, Strömholm C, Larsson M and Suzor-Weiner A 1998 *Eur. Phys. J.* D **1** 71
Yamamoto H, Matsumoto S, Okada K, Yu J and Hirakuri K 2006 *Diam. Relat. Mater.* **15** 1357–61
Yu J and Matsumoto S 2003 *Diam. Relat. Mater.* **12** 1903–7